Low-Carbon Autonomous Driving Computing via Adaptive Solar Batteries

Siyuan Zhou, Zimo Ma, Rui Tan
College of Computing and Data Science, Nanyang Technological University, Singapore

***Abstract*—Autonomous driving (AD) systems demand high computational power, leading to substantial carbon emissions from power usage. Beyond emissions related to power usage, embodied carbon from car-borne battery manufacturing is also a major concern. Repeated battery charging cycles accelerate capacity degradation, shorten battery lifespan, and ultimately necessitate battery replacement, which results in additional embodied carbon emissions. Moreover, battery degradation is affected by environmental factors such as ambient temperature and charging current, making it difficult to predict. To reduce both power usage and embodied carbon emissions, we propose LCAD, a low-carbon autonomous driving computing system via adaptive solar battery systems. LCAD harvests solar energy to reduce carbon emissions from fossil power usage. To mitigate embodied carbon from battery degradation, it dynamically switches the car-borne battery between solar charging and non-charging options. However, achieving optimal switching is challenging due to intricate interdependencies among factors such as temperature variations and fluctuating solar energy availability. To this end, we employ deep reinforcement learning (DRL) to learn an optimal switching policy. Real-world trace-driven simulation results demonstrate that LCAD significantly reduces overall carbon emissions compared with the conventional design without solar energy and battery and the other battery charging control approaches.**

***Index Terms*—Autonomous Driving, Carbon Emissions, Embodied Carbon**

I. Introduction

The recent advances in artificial intelligence (AI) strengthen the confidence in realizing autonomous driving. Various commercial autonomous driving agents (e.g., Tesla Autopilot and Baidu Apollo) have already been deployed on vehicles. However, autonomous driving leads to higher power usage. The highest level (L5) autonomous driving (AD) requires over 2,000 TOPS computing, consuming 0.75 kW of power [1]. Given Singapore's power grid carbon intensity of 467 gCO_2/kWh [2], L5 AI emits approximately 350.25 gCO_2/h. In contrast, a human driver emits only 28.7 gCO_2/h from respiration [3]. This means L5 AI has about 12 times the carbon footprint of a human driver. It generates a significant negative impact on the mission of achieving carbon neutrality and mitigating climate change, especially as autonomous driving becomes increasingly adopted.

In addition to emissions from the power grid, the embodied carbon associated with batteries and hardware also represents a significant environmental concern [4]. Embodied carbon is produced during the manufacturing, transportation, and disposal of equipment. Unlike emissions from the power grid, embodied carbon is incurred upfront and cannot be reduced after production. To mitigate the environmental impact of embodied carbon, extending the operational lifespan of components can be beneficial. A longer operational lifespan amortizes the one-time embodied carbon over a longer period of use, effectively reducing the embodied carbon emission per unit usage. Therefore, lifespan optimization serves as a potential strategy for reducing environmental impact. In autonomous driving, components such as the vehicle body and onboard computing units are often viewed to have lifespans that do not depend on usage, leaving limited opportunities for optimization. In contrast, the car-borne battery, which powers AI computations, undergoes electrochemical cycles that lead to battery degradation, making its lifespan highly dependent on usage and operational conditions. This variability in battery degradation provides an opportunity for optimization. Reducing battery degradation lowers the embodied carbon emission per usage, thereby mitigating its environmental impact.

In this paper, we propose LCAD, a low-carbon autonomous driving computing system via adaptive solar battery systems. It is designed to reduce the combined impact of power grid emissions and embodied carbon emissions arising from battery degradation. To reduce power grid emissions, LCAD uses a roof-mounted solar panel to harvest solar energy and store it in a car-borne battery that exclusively powers AI computations. Ideally, AI computations are powered entirely by carbon-free energy, eliminating the emissions associated with the use of grid electricity. However, since the amount of harvested solar energy fluctuates with weather and driving conditions, the stored energy may occasionally become insufficient to support AI computations. In such cases, the system draws power from the vehicle's electrokinetic battery, assumed to be charged by the power grid, thereby incurring power grid emissions.

However, charging cycles lead to battery degradation, which shortens lifespan, thereby leading to embodied carbon emissions. The battery degradation caused by solar charging is highly affected by battery temperature. High temperatures accelerate chemical side reactions, leading to faster degradation, while low temperatures reduce ion mobility, limiting the battery's effective capacity. As a result, charging under extreme temperatures may lead to significant battery degradation, potentially causing its embodied carbon emission per charge to exceed the emission of the power grid. To minimize overall carbon emissions, LCAD dynamically switches between charging and non-charging options for the car-borne battery, considering the impact of temperature on battery degradation while balancing the trade-off between embodied and power

2325-1301/25/$31.00 ©2025 IEEE
DOI 10.1109/RTCSA66114.2025.00030

grid carbon emission.

Achieving optimal switching is challenging due to intricate interdependencies among various factors. Battery temperature is affected not only by ambient conditions but also by the charging process, creating a feedback loop that complicates the switching decision. To this end, we employ deep reinforcement learning (DRL) to learn an effective long-term switching policy. However, the typical online training of DRL requires excessive time to converge, potentially leading to high carbon emissions during the early training phase. To address these challenges, we adopt an offline training approach that leverages data traces to train the DRL agent. Finally, the trained agent is evaluated in simulation environments.

We conduct extensive real-trace-driven simulations to evaluate the effectiveness of our proposed DRL method against three baselines. The simulation results show that our method can effectively reduce total carbon emissions by 20.4%.

II. Related Work

Many studies have focused on investigating carbon emissions. One research direction focuses on reducing system operational power usage to lower carbon emissions [5]–[7]. The study in [5] proposes a DRL-based scheduling strategy to dynamically allocate AI tasks with varying latency requirements and energy consumption across heterogeneous edge devices, reducing overall energy usage to lower carbon emissions while ensuring task deadlines are met. ECMS [6] assigns compute-intensive tasks to high-performance servers for low latency while offloading low-priority tasks to energy-efficient nodes, reducing power spikes and overall energy consumption. UPTPU [7] dynamically disables underutilized Multiply-And-Accumulate units based on batch size, eliminating unnecessary power consumption from zero-weight computations to reduce carbon emissions.

Another direction focuses on evaluating the carbon footprint of AI and identifying opportunities to reduce emissions [8]–[10]. The study in [8] proposes Spatial-Temporal Embodied Carbon (STEC) models to enhance the accuracy of embodied carbon accounting for computer systems by considering spatial and temporal variations in electricity carbon intensity. The study in [9] quantifies the carbon emissions from training and tuning large AI models based on hardware power consumption. LLMCarbon [10] estimates operational and embodied carbon emissions from the hardware used in LLM training. In contrast, our paper aims to minimize the total carbon emissions of the autonomous driving system, including both computing-related and embodied carbon emissions.

Reinforcement learning (RL) has been applied to control the system configuration in autonomous driving [11]–[13]. The study in [11] applies deep reinforcement learning to control vehicle acceleration and steering at busy roundabouts by observing map information, routing trajectories, detected objects, and historical ego states. The study in [12] uses reinforcement learning to observe vehicle speeds, positions, and lane-change behaviors, making speed and lane-change decisions to maintain steady-state autonomous driving. EC-Seg [13] employs an RL agent to switch between edge and cloud processing options to achieve high image segmentation accuracy in autonomous vehicles. Our work adopts a similar DRL-based control approach for a switching strategy to reduce carbon emissions in AD systems while considering the impact of battery temperature.

III. The Proposed Method

This section presents LCAD, which adopts a DRL agent to control battery charging for solar energy storage, aiming to minimize the total carbon emission in AD systems. In the following, we first present the system design. Next, we formulate the optimization problem and model it as a Markov Decision Process (MDP). Finally, we propose a DRL-based method to solve it.

A. System Design

We consider an AD system equipped with a solar panel. Note that a vehicle typically has two batteries: a high-voltage electrokinetic battery used for locomotion and a low-voltage auxiliary battery used for the vehicle's electronic systems [14]. In this paper, the low-voltage battery is used to store solar energy, while the electrokinetic battery is charged using power grid electricity and support the AD system only when solar energy is insufficient. Fig. 1 provides an overview of the LCAD design, which accounts for carbon emissions from two sources: embodied carbon emissions and power grid emissions.

■ **Embodied carbon:** While our system harvests carbon-free solar energy to exclusively power AI computations in the AD system, embodied carbon emissions arise from low-voltage battery degradation. The charging process induces degradation due to electrochemical side reactions and thermal stress, which are key contributors to embodied carbon emission. Charging under high battery temperatures accelerates degradation, thus increasing the embodied carbon emissions. Battery temperature is affected by ambient temperature and charging current. High ambient temperatures impair the battery's ability to dissipate heat, while high charging currents generate more internal heat due to resistive losses.

■ **Power grid carbon:** When the battery level is insufficient, AI computations fall back on electricity pre-charged from the grid, which relies on a mix of energy sources including fossil fuels, thereby resulting in power grid carbon emissions. This electricity is stored in the vehicle's electrokinetic battery. The pre-charging process refers to grid-based charging conducted in well-controlled environments. As a result, we assume this process causes negligible degradation of the electrokinetic battery. Therefore, electricity obtained through pre-charging does not lead to embodied carbon emissions.

■ **Switching:** The system has two options: charging and non-charging. The charging option harvests the solar energy which is carbon-free, while battery charging can cause embodied carbon emissions. The non-charging option avoids the embodied carbon emissions but may lead to insufficient battery

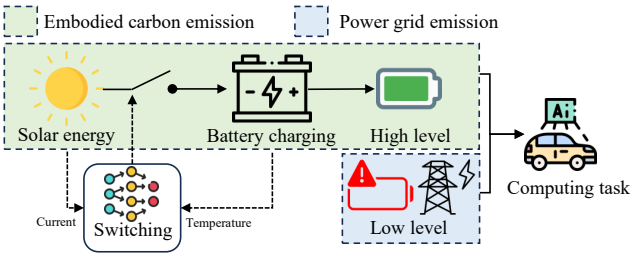

Fig. 1: Design overview of LCAD.

energy. As a result, AI computations depend on grid electricity, which introduces power grid emissions. The charging option, when operating under high battery temperatures, may result in embodied carbon emission exceeding those from power grid emissions. To minimize overall carbon emissions, including both embodied and power grid emissions, we propose a DRL-based controller that dynamically switches between charging and non-charging options, based on ambient temperature and solar charging current.

B. Problem Formulation

Time is divided into intervals with identical duration of $\tau \geq S$ minutes, which is referred to as switching period. At the beginning of switching period, called time step, the LCAD selects the charging or non-charging options for solar energy in response to the changes of two exogenous stochastic factors, including the time-varying ambient temperature, denoted by $T(t)$, and the current of solar energy, denoted by $\xi(t)$. Denote $T_k = T(k\tau)$ and $\xi_k = \xi(k\tau)$, where $k \in \mathbb{Z}_{\geq 0}$. Let $T_{t=k\tau}^{(k+1)\tau}$ and $\xi_{t=k\tau}^{(k+1)\tau}$ denote the trace of $T(t)$ and $\xi(t)$ over $t \in [k\tau, (k+1)\tau)$. At the k^{th} time step, let $\omega_k = \pi(\xi_k, T_k, \ldots, \xi_0, T_0)$ denote the switching decision based on the historical measurements $(\xi_k, T_k, \ldots, \xi_0, T_0)$. The ω_k represents the decisions, including the charging and non-charging options, which jointly affect the carbon emission during the switching period. For a time horizon of K switching periods, where K corresponds to the duration of the full battery lifespan, the switching aims to solve the policy optimization problem:

$$\pi^* = \underset{\pi \in \Pi}{\operatorname{argmin}}\ \mathbb{E}_{\xi,T}\left[\frac{1}{K}\sum_{k=0}^{K-1} C_k\left(\omega_k, \xi_{t=k\tau}^{(k+1)\tau}, T_{t=k\tau}^{(k+1)\tau}\right)\right], \quad (1)$$

where Π represents the policy space; $\omega_k = \pi(\xi_k, T_k, \ldots, \xi_0, T_0)$; $\mathbb{E}_{\xi,T}$ denotes the expectation over the two stochastic processes of $T(t)$ and $\xi(t)$; the $C_k(\cdot)$ denotes the carbon emissions in the k^{th} switching period. The objective is to find the optimal policy π^* that minimizes the carbon emissions per switching period.

C. System Carbon Emissions

The $C_k(\cdot)$ consists of two components: embodied carbon emissions and power grid carbon emissions.

1) Embodied carbon: The C_e^k denotes the embodied carbon emission in the k^{th} period and is computed as $C_e^k = \Delta C^k \cdot C_{\text{unit}} \cdot E_{\text{c}}^k$, where ΔC^k represents the battery lifespan degradation per kilowatt-hour (kWh) of solar charging, C_{unit} is the carbon emission per battery manufactured, and E_{c}^k is the amount of charged solar energy in the k^{th} period. The degradation ΔC^k is affected by the battery temperature T_{b} during the k^{th} period. We adopt a widely used empirical model [15] to simulate battery degradation as a function of temperature: $\Delta C^k = (a \cdot T_{\text{b}}^2 + b \cdot T_{\text{b}} + c) \cdot \exp(d \cdot T_{\text{b}} + e) \cdot f$, where a, b, c, d, e, and f are empirical parameters obtained from experimental data. This model indicates that charging under excessively high or low temperatures significantly increases embodied carbon emissions. The C_{unit} is related to battery materials and the manufacturing process. It is treated as a constant in this paper.

2) Power grid carbon: The power grid carbon emissions C_c^k represent the carbon emissions from pre-charged electricity used in the k^{th} period. It is computed as $C_c^k = E_p^k \cdot C_{\text{grid}}$. C_{grid} denotes the grid carbon intensity, defined as the carbon emissions per kWh of electricity generated from the grid. The value of C_{grid} varies across countries due to differences in their power generation mixes, such as reliance on coal, natural gas, or renewable energy. In this paper, we assume a fixed value for C_{grid}, as vehicles are typically operated within a single country. The value of E_p^k represents the amount of pre-charged energy used in the k^{th} period, which is defined as $E_p^k = \max(0, E_{\text{task}} - E^k)$. The E_{task} refers to the energy required for AI computation. It is assumed to be a fixed value throughout the operation. The E^k represents the available solar energy stored in the battery in the k^{th} period. The decision to charge using solar energy is made by comparing $\Delta C^k \cdot C_{\text{unit}}$ with C_{grid}, in order to select the option with lower carbon emissions.

D. Battery Temperature

The battery temperature T_{b} is affected by two dynamic environmental factors: the ambient temperature T and the solar charging current I. The charging current generates heat through internal resistance, converting electrical energy into thermal energy. Moreover, the ambient temperature T affects the rate at which the battery dissipates heat. The T_{b} is determined by the combined effects of internally generated heat and externally dissipated heat.

In this paper, we simulate the battery temperature at each time step using the following first-order heat transfer equation: $T_{\text{b}}[k+1] = T_{\text{b}}[k] - g(T_{\text{b}}[k] - T[k+1]) + hI^2[k+1]$ where $T_{\text{b}}[k]$ represents the battery temperature at timestamp k, $T[k+1]$ is the ambient temperature, and $I[k]$ denotes the charging current [16]. This equation indicates that the battery temperature at time step k+1 is jointly determined by the ambient temperature and charging current at time step k+1, as well as the battery temperature at time step k. This equation is applied iteratively to simulate the battery temperature dynamics over time. The parameters g and h depend on the battery's physical characteristics, including its size, thermal properties, and cooling conditions. It is difficult to predict $T_{\text{b}}[k+1]$ due to its joint dependence on multiple dynamic factors. To address the challenge, we employ a DRL-based approach for making charging decisions under ambient temperature and charging current uncertainty.

E. MDP Formulation

System state: At time step k, the system state, denoted by $\boldsymbol{x}_k$, is a vector $\boldsymbol{x}_k = [T_{\mathrm{b}}^k, T_k, I_k, E_k]$, where T_{b}^k represents the battery temperature in the last period, I_k represents the harvested solar charging current in the last period, T_k represents the ambient temperature at the beginning of the k^{th} period, and E_k represents the remaining solar energy in the battery at the beginning of the k^{th} period. A value of T_{b}^k that is too high or too low can accelerate battery degradation, leading to large embodied carbon emissions. A large T_k indicates that the battery dissipates heat more slowly. A larger I_k represents a higher charging current, which can increase the battery temperature at time step k. A large value of E_k suggests that the battery has enough stored solar energy, allowing LCAD to avoid using pre-charged grid electricity to reduce power grid carbon emission.

Switching action: The switching action, denoted by $a_k \in \{0, 1\}$, represents the choice between charging and not charging options to be executed in the current period.

Reward function: When an action a_k is performed at the current time step and the system state is $\boldsymbol{x}_k$, let $C_k(\boldsymbol{x}_k, a_k)$ denote the total carbon emissions. $C_k(\boldsymbol{x}_k, a_k)$ varies in response to changes a_k and $\boldsymbol{x}_k$.

F. DRL Approach

We adopt the learning framework of a DRL algorithm, called the proximal policy optimization (PPO) [17] to learn the optimal switching policy. PPO directly learns from a stochastic distribution, leading to more effective exploration, and adopts a clipping mechanism to improve efficiency compared with Deep Q-Networks and Trust Region Policy Optimization. Under the typical setting, a PPO agent learns the optimal policy during the online interactions with the controlled system. However, for the formulated switching problem, the online DRL scheme faces a challenge, as PPO agent training requires a long time to learn the policy, which may lead to unnecessary carbon emissions due to trials and errors. To address this challenge, we adopt an offline training approach, as illustrated in Fig. 2, which consists of three steps. First, we collect real data traces from the environment. Second, we use the collected data and a widely used empirical model to drive the offline training of the PPO agent. Third, the trained PPO agent is evaluated in simulation to make switching decisions.

IV. Evaluation

This section presents the experiment settings and execution performance of LCAD.

A. Experiment Setup

We use over two hours of self-collected, real-world solar energy traces to simulate the available solar energy in an autonomous driving system. Specifically, to collect these traces, we built a solar energy harvesting testbed, as shown in Fig. 3. The testbed comprises monocrystalline solar panels and a maximum power point tracking (MPPT) charge controller, which supports up to 10 A of current to optimize power

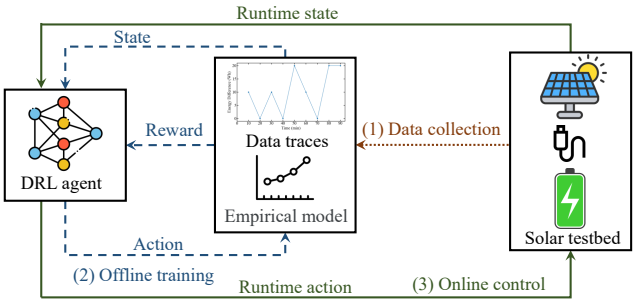

Fig. 2: Workflow of DRL-based switching.

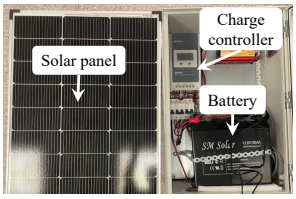

Fig. 3: Solar panel system.

TABLE I: Parameter settings for simulation

Param	Value
a	8.581×10^{-6}
b	-5.102×10^{-3}
c	0.7589
d	-6.7×10^{-3}
e	2.344
f	1.5
g	0.208
h	0.042

extraction and regulate the charging process. The MPPT charge controller is capable of recording harvested solar energy data, including the energy and charging current, at 10-minute intervals. A lithium iron phosphate battery is included to store the harvested solar energy. To emulate realistic driving conditions, we mount a 100 W solar panel on a lorry. The panel lies flat horizontally without any sun-tracking mechanism. The lorry continuously travels through various environments such as tunnels, overpasses, and open streets, at speeds of up to 60 km/h for 90 minutes on a sunny day.

We use over 7,030 minutes of vehicle temperature data from a public dataset to simulate the ambient temperature in our simulation [18]. The PPO agents are implemented using the Python library Stable-Baselines3 version 2.4.1. We assume each autonomous driving system is deployed on a Jetson Orin device, whose peak power consumption is 60 Wh per hour. Accordingly, we set the energy consumption of the AD system to 60 Wh per hour. The carbon emission per battery manufactured C_{unit} is set to 150 kgCO_2 [4]. The C_{grid} is set to 367 gCO_2/kWh based on 2024 data from the United States [19]. The corresponding hyperparameter settings for battery degradation and the heat transfer equation are presented in Table I.

B. DRL Training Performance

We build a PPO-based DRL model with an input layer, two hidden layers and an output layer. The two hidden layers have 64 and 64 ReLUs, respectively. The Adam optimizer with a learning rate of 10^{-4} is used for training. The PPO agent is trained with a likelihood ratio clipping set at 0.25 to balance stability during the learning process. Moreover, the switching period τ is set to 10 minutes. At the beginning of every period, the DRL agent observes a system state $\mathbf{x}$, including the

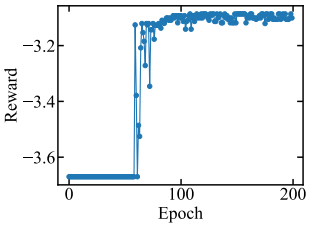

Fig. 4: Training results.

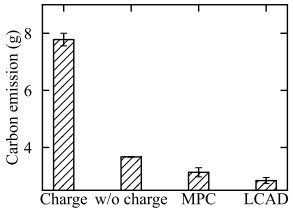

Fig. 5: Execution results.

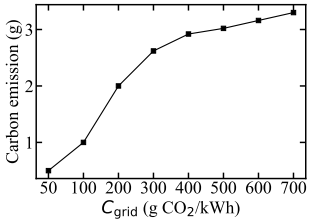

Fig. 6: Performance under different C_{grid}.

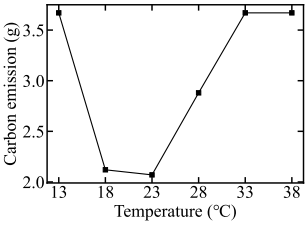

Fig. 7: Performance under different ambient temperature.

battery temperature, ambient temperature, charging current, and remaining solar energy. Then, it selects an action $a \in \{0, 1\}$ to choose the charging or no charging. Subsequently, the embodied carbon and computing carbon emissions are utilized to compute intermediate reward values.

The offline training is conducted for 200 episodes, each of which includes $1,000$ switching periods. Fig. 4 shows the PPO training traces of the rewards with various state inputs. Along the training episodes, the reward trace increases and then becomes flat under different inputs. The results show that the PPO agent can converge after a certain number of training episodes.

C. Execution Performance

To assess the efficacy of the proposed LCAD system, we compare our LCAD with three baseline methods as follows: *w/o charge:* The vehicle does not charge its battery using solar energy and always relies on power grid electricity to support AI computation tasks. *Charge:* The vehicle continuously charges its battery using solar energy. *MPC:* The decision to charge or not is determined using a model predictive control (MPC) strategy, a widely adopted method for solving sequential decision-making problems [20]. MPC leverages autoregressive moving average (ARMA) models to forecast ambient temperature, solar energy, and solar charging current. These forecasts are used to estimate future carbon emissions over a horizon length of 20 switching periods. The action that yields the lowest carbon emissions in the immediate next period is selected.

Fig. 5 presents the average carbon emission in every 10 minutes for the proposed LCAD and two baseline approaches over a 10000 switching period. The w/o charge approach can achieve 3.67 gCO_2 across all periods. The *charge* approach results in the highest carbon emissions of 7.78 gCO_2, as continuous charging can increase battery temperature and accelerate battery degradation, leading to higher embodied carbon emissions. Compared with the three baseline methods, our approach achieves the lowest carbon emissions and outperforms the *w/o charging* approach by over 20.4%. This improvement is attributed to the DRL agent's ability to make informed charging decisions that avoid severe battery degradation when the battery temperature is high.

Moreover, on the Jetson Orin autonomous driving computer unit, the MPC controller takes 718 seconds on average to determine an action, while the DRL controller takes only 0.005 seconds. Since each switching period is only 600 seconds, the MPC approach violates the timeliness requirements. Given that autonomous driving is a resource-constrained application, the MPC method is unsuitable for practical deployment. Assuming a 60 W power draw, the 718-second computation adds approximately 11.97 Wh per decision, resulting in around 4.39 g of CO_2 emissions, which may even exceed the carbon savings achieved by the decision. This indicates that the MPC approach introduces additional carbon emissions.

D. Evaluation in Different Power Grid Emission

We further conduct experiments to investigate the performance of LCAD under different power grid carbon intensities. Since the value of C_{grid} varies across countries, we simulate a range of C_{grid} values from 50 to 700 gCO_2/kWh, with an interval of 100. This range reflects real-world grid carbon intensities. For example, France has a low grid emission of 56 gCO_2/kWh due to its reliance on nuclear energy, while India reaches up to 700 gCO_2/kWh owing to its coal-dominated power generation [21]. For each simulated scenario, we train a DRL agent and evaluate its performance under the corresponding grid emission setting.

Fig. 6 presents the average carbon emissions of LCAD under different C_{grid} values. When C_{grid} is 200 gCO_2/kWh, the average carbon emission is as low as 1 g, because the DRL agent consistently selects the non-charging option. When C_{grid} exceeds 500 gCO_2/kWh, the carbon emissions remain nearly constant. This is because the DRL agent always chooses to charge, making the system less sensitive to further increases in grid emission. Therefore, LCAD can provide significant carbon reduction benefits in countries where C_{grid} is higher than 300 gCO_2/kWh.

E. Evaluation in Different Ambient Temperature

We further conduct experiments to evaluate the performance of LCAD under different ambient temperature conditions. Based on a public vehicle temperature dataset with artificial biases, we generate temperature traces with varying average values to emulate ambient conditions reflecting real-world seasonal and geographical variations. Fig. 7 presents the average carbon emissions of LCAD in each period under various average ambient temperatures. When the average temperature is below 13 °C or above 33 °C, the carbon emission reaches 3.67 g, indicating that LCAD consistently decides not to charge using solar energy to avoid severe battery degradation.

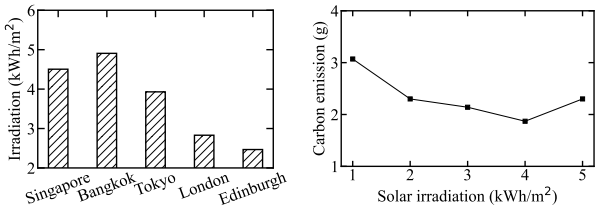

(a) Solar irradiation in varies cities.

(b) Carbon emissions of LCAD under varying solar irradiation levels.

Fig. 8: Impact of solar irradiation on LCAD performance.

Therefore, LCAD provides carbon reduction benefits when the ambient temperature is between 13 °C and 33 °C.

F. Evaluation in Different Solar Irradiations

The harvested energy and charging current of solar panels may vary across cities at different latitudes. Solar irradiation is closely related to the performance of harvested energy from solar panels [22]. Note that the solar irradiation is highly affected by latitude. Due to the Earth's axial tilt, cities at lower latitudes receive higher solar irradiance. For instance, cities near the equator receive more consistent solar irradiation compared with those located closer to the poles. We collect the solar irradiation data in five cities with varying latitudes from the Global Solar Atlas [23], which is a global solar energy platform.

Fig. 8(a) presents the latitudes of five cities located at approximately sea level and their corresponding average daily global horizontal irradiation over a 10-year period. As latitude increases, solar irradiation decreases due to reduced direct sunlight. For example, the solar irradiation in Bangkok (latitude 13.45°) is 1.98× that of Edinburgh (latitude 55.57°). To further analyze the effectiveness of LCAD under varying solar irradiations, we simulate a series of harvested energy traces by scaling the original trace to different irradiation levels, ranging from 1 to 5 kWh/m^2 in steps of 1. Specifically, we apply a uniform scaling method [24], adjusting the harvested energy and charging current proportionally based on the target solar irradiation level. To better understand the impact of solar energy, we adopt ambient temperature traces with an average value of 23 °C, as used in § IV-E, to evaluate system performance.

Fig. 8(b) presents the average carbon emission of each switching period under different solar irradiation. When the average solar irradiation increases from 1 to 4 kWh/m^2, the carbon emissions gradually decrease, as LCAD is able to harvest more solar energy to power the autonomous driving system. However, when the irradiation reaches 5 kWh/m^2, carbon emissions rise. This is because excessive solar energy results in a higher charging current, which can increase battery temperature and induce additional embodied carbon emissions due to battery degradation. These results indicate that while increasing solar irradiation generally benefits carbon reduction, effective thermal management becomes crucial under high solar input conditions.

G. System Carbon Reduction

We further evaluate the total carbon emissions of the LCAD system against a conventional design that relies solely on grid electricity for AI computation across different countries with different C_{grid}, without solar integration. The generation of solar energy is a carbon-free process, but the manufacturing of solar panels results in carbon emissions. The embodied carbon of a monocrystalline silicon solar panel is measured at 127.3 kgCO_2 per square meter [25]. We assume that both the vehicle and the integrated solar panel have a lifespan of 10 years. During this period, the vehicle is assumed to operate for 5 hours per day. We simulate the LCAD system over a 10-year period, incorporating the embodied carbon of the solar panel, and compare the carbon emission with those of the conventional design.

Table II presents the total carbon emissions of the LCAD system and the conventional design across different countries [21]. Under USA's C_{grid}, the LCAD system produces lower total carbon emissions (382.1 kgCO_2) over a 10-year period compared with the conventional grid-only design (401.8 kgCO_2). Under Singapore's C_{grid}, the LCAD system emits 411.9 kgCO_2, compared with 511.4 kg from the grid-only design. Under China's higher C_{grid}, LCAD emits 426.1 kgCO_2, compared with 637.3 kg from the grid-only design, achieving a 33.1% reduction. These results indicate that LCAD provides greater carbon savings in regions with higher grid carbon intensity.

TABLE II: Total carbon emissions over a 10-year period across countries

Country	C_{grid}	**Approach**	**Emissions (kgCO_2)**	**Saving (%)**
USA	367	LCAD	382.1	4.9
		grid-only	401.8	
Singapore	467	LCAD	411.9	19.5
		grid-only	511.4	
China	582	LCAD	426.1	33.1
		grid-only	637.3	

V. Conclusion

This paper presents LCAD, a low-carbon autonomous driving computing system via adaptive solar battery systems. In particular, this paper considers the embodied carbon emissions of the autonomous driving system. We formulate an MDP to minimize the carbon emissions of autonomous driving, considering both power grid emissions and the embodied carbon associated with battery degradation, under dynamic variations in solar energy availability and ambient temperature. To address this challenge, we apply deep reinforcement learning to learn an optimal solar energy charging policy. Our trace-driven simulations demonstrate that LCAD can effectively reduce the carbon emissions of autonomous driving and achieves lower total emissions compared with three charging control baseline approaches and the conventional design without using solar energy and battery.

ACKNOWLEDGMENT

This research is supported by Singapore Ministry of Education under its AcRF Tier-1 grant RT14/22.

REFERENCES

[1] "Next-generation gpu." [Online]. Available: https://wccftech.com/nvidia-next-gen-gpuarchitecture-powered-orin-soc-announced/

[2] "Sg electricity carbon." [Online]. Available: https://app.electricitymaps.com/zone/SG/72h/hourly

[3] M. Li, G. Bekö, N. Zannoni, G. Pugliese, M. Carrito, N. Cera, C. Moura, P. Wargocki, P. Vasconcelos, P. Nobre, and N. Wang, "Human metabolic emissions of carbon dioxide and methane and their implications for carbon emissions," *Science of the Total Environment*, vol. 833, 2022.

[4] Ö. Andersson and P. Börjesson, "The greenhouse gas emissions of an electrified vehicle combined with renewable fuels: Life cycle assessment and policy implications," *Applied Energy*, vol. 289, p. 116621, 2021.

[5] S. Zhu, K. Ota, and M. Dong, "Green ai for iiot: Energy efficient intelligent edge computing for industrial internet of things," *IEEE Transactions on Green Communications and Networking*, vol. 6, no. 1, pp. 79–88, 2021.

[6] Z. Zhou, M. Shojafar, J. Abawajy, H. Yin, and H. Lu, "Ecms: An edge intelligent energy efficient model in mobile edge computing," *IEEE Transactions on Green Communications and Networking*, vol. 6, no. 1, pp. 238–247, 2021.

[7] P. Pandey, N. D. Gundi, K. Chakraborty, and S. Roy, "Uptpu: Improving energy efficiency of a tensor processing unit through underutilization based power-gating," in *2021 58th ACM/IEEE Design Automation Conference*, 2021, pp. 325–330.

[8] X. Zhang, Y. Yang, and D. Wang, "Spatial-temporal embodied carbon models for the embodied carbon accounting of computer systems," in *Proceedings of the 15th ACM International Conference on Future and Sustainable Energy Systems*, 2024, pp. 464–471.

[9] E. Strubell, A. Ganesh, and A. McCallum, "Energy and policy considerations for modern deep learning research," in *Proceedings of the AAAI conference on artificial intelligence*, vol. 34, no. 09, 2020, pp. 13 693–13 696.

[10] A. Faiz, S. Kaneda, R. Wang, R. C. Osi, P. Sharma, F. Chen, and L. Jiang, "Llmcarbon: Modeling the end-to-end carbon footprint of large language models," *The 12th International Conference on Learning Representations*, 2024.

[11] J. Chen, B. Yuan, and M. Tomizuka, "Model-free deep reinforcement learning for urban autonomous driving," in *2019 IEEE intelligent transportation systems conference*, 2019, pp. 2765–2771.

[12] C.-J. Hoel, K. Driggs-Campbell, K. Wolff, L. Laine, and M. J. Kochenderfer, "Combining planning and deep reinforcement learning in tactical decision making for autonomous driving," *IEEE transactions on intelligent vehicles*, vol. 5, no. 2, pp. 294–305, 2019.

[13] S. Zhou, D. Van Le, and R. Tan, "Ecseg: Edge-cloud switched image segmentation for autonomous vehicles," *Annual IEEE International Conference on Sensing, Communication, and Networking*, 2024.

[14] "12v battery." [Online]. Available: https://www.varta-automotive.com/knowledge/articles/article-details/12-volt-batteries-in-electric-cars

[15] A. Thingvad, L. Calearo, P. B. Andersen, and M. Marinelli, "Empirical capacity measurements of electric vehicles subject to battery degradation from v2g services," *IEEE Transactions on Vehicular Technology*, vol. 70, no. 8, pp. 7547–7557, 2021.

[16] A. Abdollahi, X. Han, G. Avvari, N. Raghunathan, B. Balasingam, K. R. Pattipati, and Y. Bar-Shalom, "Optimal battery charging, part i: Minimizing time-to-charge, energy loss, and temperature rise for ocv-resistance battery model," *Journal of Power Sources*, vol. 303, pp. 388–398, 2016.

[17] J. Schulman, F. Wolski, P. Dhariwal, A. Radford, and O. Klimov, "Proximal policy optimization algorithms," *arXiv*, 2017.

[18] "Temperature data." [Online]. Available: https://www.kaggle.com/datasets/atechnohazard/battery-and-heating-data-in-real-driving-cycles/data?select=TripA01.csv

[19] "Us carbon." [Online]. Available: https://www.eia.gov/tools/faqs/faq.php

[20] Y. Ma, F. Borrelli, B. Hencey, B. Coffey, S. Bengea, and P. Haves, "Model predictive control for the operation of building cooling systems," *IEEE Transactions on control systems technology*, vol. 20, no. 3, pp. 796–803, 2011.

[21] "World carbon intensity." [Online]. Available: https://ourworldindata.org/grapher/carbon-intensity-electricity

[22] J. Peng, L. Lu, and H. Yang, "Review on life cycle assessment of energy payback and greenhouse gas emission of solar photovoltaic systems," *Renewable and sustainable energy reviews*, vol. 19, pp. 255–274, 2013.

[23] "Atlas." [Online]. Available: https://globalsolaratlas.info/map

[24] "Scaling." [Online]. Available: https://en.wikipedia.org/wiki/scaling-geometry

[25] Y. Gan, A. Elgowainy, Z. Lu, J. C. Kelly, M. Wang, R. D. Boardman, and J. Marcinkoski, "Greenhouse gas emissions embodied in the us solar photovoltaic supply chain," *Environmental Research Letters*, vol. 18, no. 10, p. 104012, 2023.